Electronic Supplementary Material (ESI) for Lab on a Chip.

Supplementary materials

S1 Fluid dynamic analysis

S1.1 Methods

S1.1.1 Computational fluid dynamic analysis

To evaluate the influence of device geometry, cell size and media flow rate on the single cell retention inside the U-shaped trap, four single-well models, with a fixed cell in the trap were created using Ansys ICEM CFD 14.0 (Ansys®) and assessed using Ansys CFX 14.0 (Ansys®). The channel height, well depth and cell diameter of four models tested are listed in Table S1. The single-well model (see Figure S1a) consisted of a 1.06 mm wide channel on top of a well (1-mm in diameter), a 27-µm wide U-shaped trap, a 10-µm wide channel and a sphere (representing a cell, either 14 µm or 24 µm in diameter) fixed on the floor of the trap.

The Reynolds numbers studied in all models were 0.0005, 0.005, 0.0124, 0.0248, 0.0496 and 1.8. The relevant flow rates (q) at the inlet ports were either 0.0125, 0.126, 0.312, 0.624, 1.248 and 45.286 µL/min (for models 50-50, 50-250, and 50-50L) or 0.0131, 0.132, 0.327, 0.654, 1.307, and 47.44 µL/min (for model 100-50). All boundaries except inlet and outlet were set as non-slip walls. To determine the critical Re for lifting the cell out of the trap in model 50-50, the Re= 10, 11, 12, 15, and 20 were studied. A large cell with the diameter of 24 µm (referred to as model 50-50L) was employed to study a) the influence of the cell size on the fluid induced forces on the cell and b) if a larger cell could still be retained in the trap (Figure S1c). The full-hex mesh was employed for all models (Figure S1 b and c).

Table S1. The channel height, well depth and cell diameter of four models for simulation.

Models	Channel height (µm)	Well depth (µm)	Cell diameter (µm)
50-250	50	250	14
50-50	50	50	
100-50	100	50	
50-50L	50	50	24

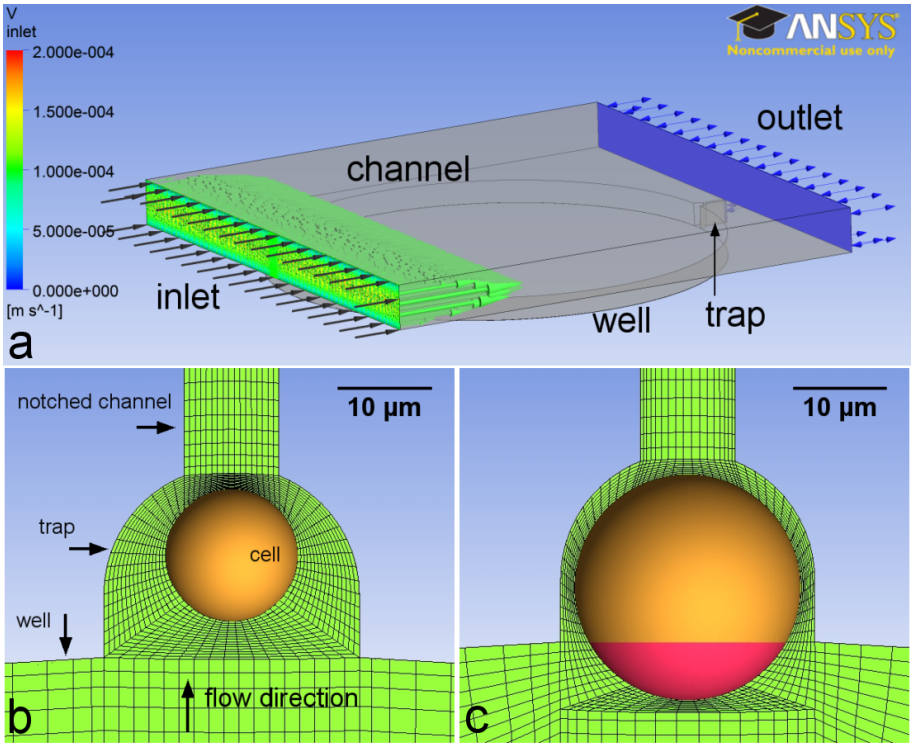

Figure S1 (a) The single well model with the top flow channel, bottom well, U-shaped trap and the fixed sphere. The top views of the full hex mesh with cells that are either 14-µm (b) or 24-µm (c) in diameter inside the traps.

The optimal convergence criteria and total element number (grid size) may dramatically reduce the simulation time without compromising the accuracy of the result. Therefore, the convergence criteria, root mean square (RMS), ranging from 1×10^{-6} to 1×10^{-12} was studied using model 100-50 to acquire the suitable RMS. The total element number was varied from 0.21 to 1.9×10^{6} in the model 50-50 to acquire a grid-independent simulation. Following the optimisation, double precision with the convergence criteria of RMS=10^{-10} and total element number of around 1×10^{6} were applied in all models to guarantee the accuracy of the fluid-induced forces and torques.

The single well model for the CFD analysis is shown in Figure S1a. The results of convergence and grid independent studies were shown in Figure S2. It is found that when RMS<10^{-8}, the simulation is independent of the RMS and when total elements number is ⩾ 5.5 × 10^5, the simulation is grid independent. All other simulations in this study applied RMS=10^{-10} and 1 × 10^6 elements per model to guaranty the accurate values of the fluid induced forces and torques.

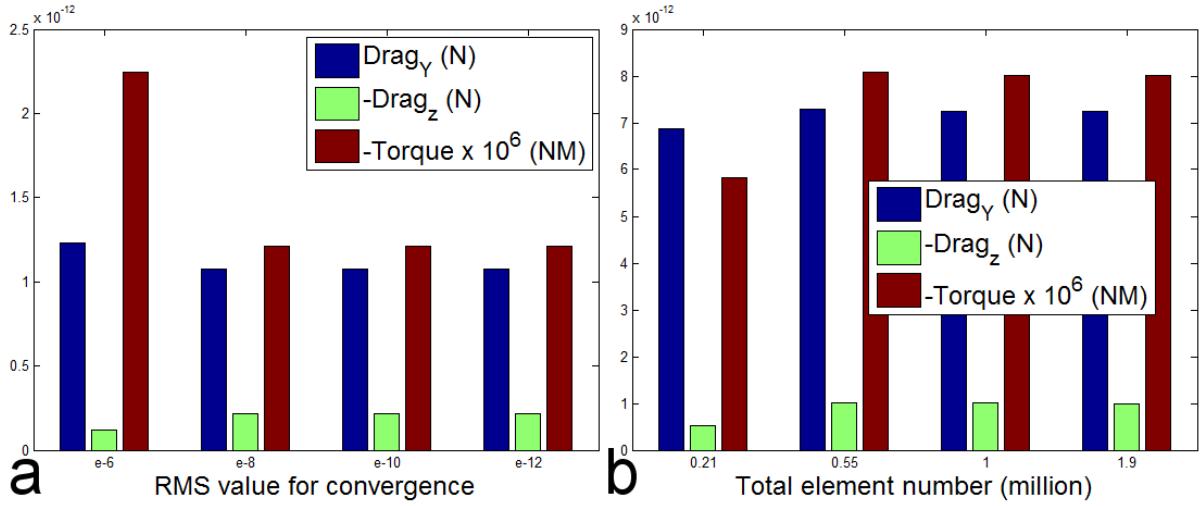

Figure S2. (a) The various quantities calculated using different convergence criteria. (b) various quantities acquired using models with distinct element densities. When RMS<10^{-8} and the total element number is larger than 0.55 × 10^6, the drag and the torque on the cell do not vary significantly.

S1.1.2 MicroPIV

Micro Particle Image Velocimetry (μPIV) has been extensively applied to measure instantaneous fluid velocity inside microfluidic devices. In this study, the fluid flow on the mid-planes of both the well and the flow channel in the Device 1 mm well was characterised using μPIV. Following degassing and rinsing using DI water, the microdevice was placed on an inverted microscope (Nikon TE2000-U) equipped with a μPIV system (PCO Sensicam CCD camera and ND:YAG laser light source). The microscope focused on the mid-planes of either the channel or the well by determining the top and bottom and moving halfway back. The fluorescent polymer microspheres (Duke Scientific Corp., Cat No. R700) with the diameter of 0.71 μm were diluted in DI water with the volume ratio of 1:1000 (microsphere solution: water). The diluted microsphere solution was then injected into the Device 1 mm at the flow rates of 1, 5, 10, 15 and 20 μL/min using a syringe pump. The relevant timing between two laser pulses was set to 60, 9, 7, 4 and 2 ms for the flow rates of 1, 5, 10, 15 and 20 μL/min. Fifty image pairs were recorded for each flow rate. The images were processed to

calculate the displacement of microspheres as function of time and therefore acquire the mean velocity of the fluid in a 20 × 20 μm region in the centre of the mid-plane of both the flow channel and the bottom well.

S1.2 Results and discussion

S1.2.1 CFD

The CFD analysis was applied to quantitatively study the fluid-induced forces on the cell placed inside the trap when the cell size, ratio of the well depth and flow channel height and Re were varied. The z-component of the drag (Dz) and y-component of the shear stress (τ_y) on the cell in all models when Re varied from 5 $\times 10^{-4}$ to 1.8 are shown in Figure S3 d and e. Under the same Re, when cell size increases, the fluid induced force (Dz) becomes larger; when the well become deeper, the fluid induced force decreases, while when height of the flow channel is larger, the fluid induced force is even smaller. The y- and z- components of the drag (Dy and Dz), the x-component of the torque (Tx) and the shear stress in y direction (τ_y) can be related to a linear equation $f(Re) = aRe$, where $f(Re)$ is the relevant quantity (Dy, Dz, Tx or τ_y), Re is the Reynolds number and a is a constant (see Table S2). The negative value indicates that the direction of the quantity is in the negative direction of the relevant axis (see Figure S3a for the coordinate). From Table S2, all quantities can be estimated when 5 $\times 10^{-4}$ ≤Re≤1.8. It is also found that when the Re is constant, the fluid induced force is dependent on the size of the cell to the largest extend. The Dz always points down to the well bottom and Dy is always in the +y direction (points to the downstream well wall). A larger cell partly placed inside the trap (in model 50-50L) is also subject to the fluid induced forces and torque with the same directions as those of a smaller cell (in model 50-50). Dz on the cell in model 50-50 when 5 $\times 10^{-4}$ ≤Re≤20 is shown in Figure S3f. The z-component of the drag becomes positive from negative when Re rises from 11 to 12. A mechanical equilibrium analysis was carried out to further understand the single cell trapping from mechanistic point of view. The schematic of forces and the fluid induced torque are shown in Figure S3c. Taking model 50-50 as an example, when Re=1.8, Dy=5.5 × 10^{-10} N, Dz=-5.8 × 10^{-11} N, and Tx =-6.3× 10^{-16} Nm, assuming the density of the cell is 1035.7 kg/m3 33. The difference (G-Fb) between the gravitational force G and buoyancy force Fb is -5.0× 10 $^{-13}$ N (pointing downwards to the well bottom). The cell is subjected to a Dy, pointing to the well wall, G-Fb+Dz (~ 5.8 × 10^{-11} N) as well as normal reaction forces from the floor and vertical wall to balance the other forces (G-Fb+Dz and Dy). Therefore, all the forces on the

cell are balanced and the cell stay still when Re=1.8. From the simulation, it is predicted that the cell in all models could be mechanically stabilised in situ when Re ranges from 0.0005 to 1.8.

Table S2. The constants (a) for linear regression analysis of all quantities (R^2=1) when $5 \times 10^{-4} \leq Re \leq 1.8$.

Model	Constant			
	Dy × 10^{-11} (N)	Dz × 10^{-12} (N)	Tx × 10^{-17} (N·M)	τ_y (Pa)
50-250	27.48 ±0.02	-63.34±0.04	-24.38±0.02	425.4±0.4
50-50	30.75±0.05	-32.28±0.29	-35.08 ±0.1	424.2±1
100-50	4.616±0.01	-7.85±0.049	-5.382±0.018	57.81±0.13
50-50L	111.4±0.3	-115.9±1.5	-139.5±1.5	391.4±1

As shown in Figure S3f, the Dz on the cell is -1.5 × 10^{-11} N and 1.1 × 10^{-11} N when Re is equal to 11 and 12, respectively. When Re=12, Dz is 12 times larger than G-Fb. The cell will thus be lifted out of the trap due to the large positive Dz. This indicates that the critical Re for cell removal from the well is between 11 and 12. When the Re is smaller than critical Re, the cell can be stably retained in the trap.

S1.2.2 µPIV analysis

The velocity vectors on the mid-plane of two adjacent wells (Figure S3i) are shown in Figure S3h. The fluid flows from the upstream well through the 10-µm wide microchannel into the downstream well. This flow is also confirmed by the streamlines from the CFD analysis (see Figure S3a and b). The fluid velocity in the microchannel is smaller than that in the middle of the microwell.

The relationship between the mean velocity v (m/sec) acquired from the µPIV and the flow rates q (µL/min) at the inlet ports were further studied using linear regression analysis:

$$v = c \times q \tag{1}$$

, where c is a constant and estimated as 1.632 × 10^{-4} ± 5.0 × 10^{-6} (R^2=0.998) and 4.464 × 10^{-5} ± 3.34 × 10^{-6} (R^2=0.991) for the channel and the well, respectively. The mean velocity on the well mid-plane is thus equal to 27.4% of the mean velocity on the flow channel mid-plane ($v_{\text{well}} = 0.274 v_{\text{channel}}$).

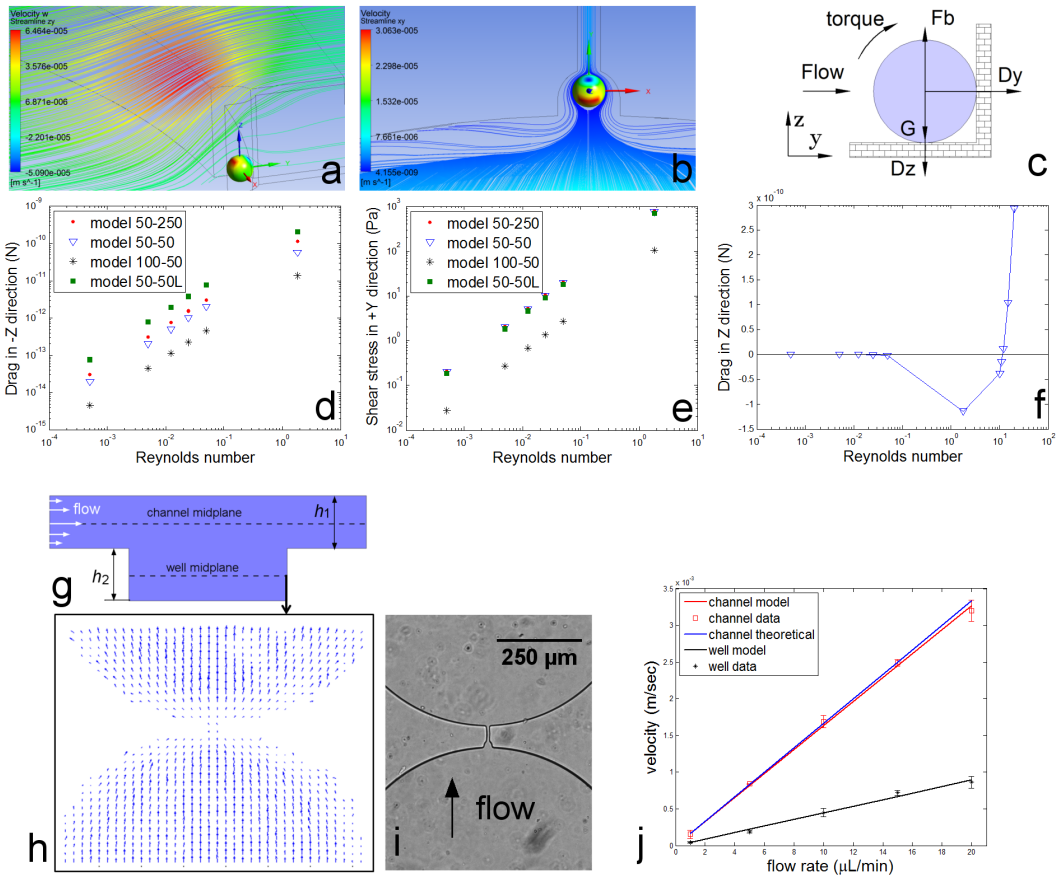

Figure S3. Side (a) and top (b) views of the streamlines on a section passing the cell centre in the model 100-50 when Re=0.025. (c) A mechanical equilibrium analysis of the cell in the model. The cell is assumed to be a rigid sphere. Fb is the buoyancy force of the cell. G is the gravitational force. Dy and Dz are the drag components in y and z directions, respectively (see Figure S3 a for the coordinates). The z-component of the drag (d) and y-component of the shear stress (e) on the cell in all models when Re varied from 5×10^{-4} to 1.8. The z-component of the drag (f) on the cell in model 50-50 when $5\times10^{-4}\leqslant Re\leqslant 20$. The z-component of the drag becomes positive from negative when Re rises from 11 to 12 (all microspheres were displaced from the traps). (g) The schematic drawing of the mid-planes where the flow velocity was measured using microPIV. (h) The vector plot of velocity on the well midplane of two adjacent wells as shown in (i). (j) The fluid velocity on the midplane of the channel (squares) and the well (stars) at various flow rates. The linear regression model of the velocity in the channel (dash line) and well (dash-dot line). The velocity in the channel (solid line) was calculated from equation 1.

To prove the accuracy of the micro PIV experiment, the velocity (v_t) on the mid-plane of the channel was calculated by:

$$v_t = q/[w\times(h_1 + h_2)] \tag{2}$$

, where w is the width of the flow channel, h_1 and h_2 (see Figure S3g) are the depth of the channel and the well, respectively. As shown in Figure S3j, the theoretical velocity v_t is not significantly different from the $v_{channel}$ (channel data). The velocity in the centre of the mid-

plane of the well can thus be predicated from the inlet flow rate and the device dimension as below:

$$v_{\text{well}} = 0.274 v_{\text{t}} = 0.274 \times q/[w \times (h_1 + h_2)] \quad (3)$$

S2 The microfluidic enclosure

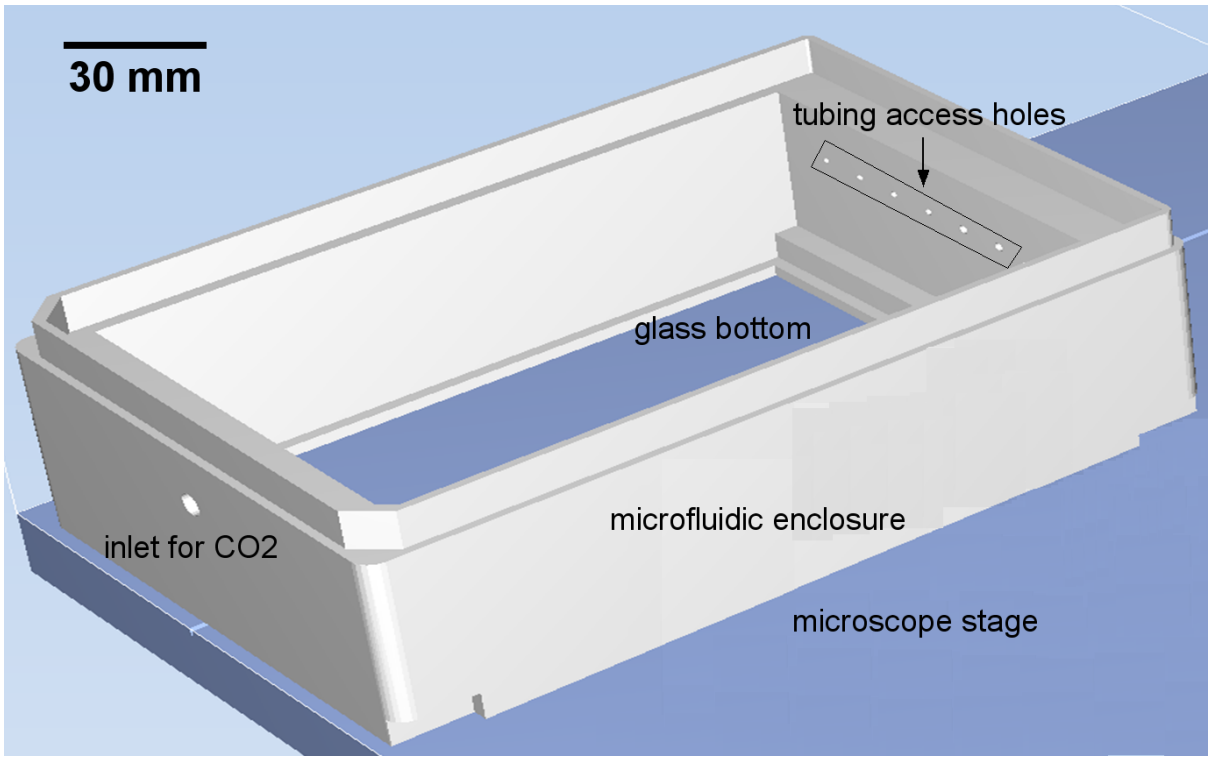

Figure S4 The 3D drawing of the microfluidic enclosure. The microfluidic device was fixed on the glass bottom inside the enclosure. The enclosure was mounted on the stage of the time-lapse microscope. A lid of a standard well plate was used to cover the enclosure. CO_2 was injected through tubing and the inlet hole into the enclosure. All the tubing of the microfluidic device passes through the tubing access holes.

S3 Cell synchronisation

To understand if the heterogeneity of single cell growth is dominated by the cycle status of cells when they were loaded into the device, the HDFs were synchronised to G0/G1 phases using serum starvation. After cultured in low-serum synchronization medium (DMEM + 0.5% FBS and 1% P-S) for 26 hours, 89.3% cells were synchronised to G0/G1 (see Figure S6). These synchronised cells were further cultured in Device '1-27' from the single cell starting point to study the cell growth heterogeneity.

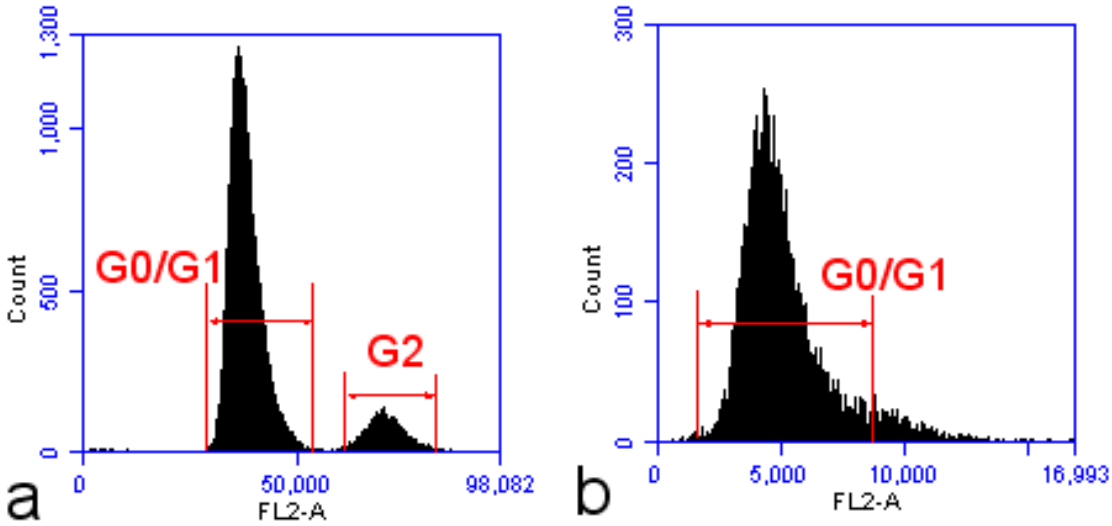

Figure S5 The cell cycles of normal growing (a) and synchronised (b) HDF. The first peak of the left figure represents the cells in G0/G1 phase.

S4 The single microsphere trapping

The below image shows the automatic segment and counting of the microsphere trapped in the microdevice using the Matlab code.

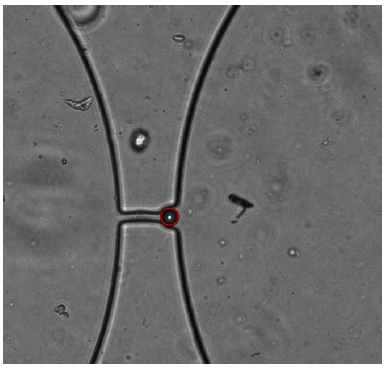

Figure S6 The automatic segmentation of single sphere (in the red circle) retained in the U-shaped trap. The sphere is accurately differentiated from the background noise by the Matlab code.

S5 Human dermal fibroblast growth study

S5.1 Aim

Compare the growth of both synchronised and normal growing human dermal fibroblast (passage 12) population in DMEM with either 10% or 30% FBS.

S5.2 Methods

S5.2.1 Cell seeding

Human dermal fibroblasts (passage 11) were reseeded into two T75 flasks. Cells (synchronisation group) in one flask was cultured in 10 ml DMEM with 0.5% FBS and 1% PS for 25 hours. Cells (normal growing group) in another flask were fed with DMEM with 10% FBS and 1% PS for 25 hours. Then cells in both groups were trypsinised and reseeded into 12 well plate . The cell seeding density was 2000 cells per well and the surface area of each well was 4 cm2. The cells were cultured in DMEM (1ml per well) with either 10% or 30% FBS (see Table).

Table S3 Culture conditions of both synchronised and normal growing cells.

Group ID	Cells	FBS concentration	Methos	Cell number ($\times 10^3$)
A1	Synchronised	10%	Growth curve study	76.3
A2			End point study	131.9
B1		30%	Growth curve study	240.8
B2			End point study	371.9
C1	Normal growing	10%	Growth curve study	32.9
C2			End point study	93.8
D1		30%	Growth curve study	187.5
D2			End point study	371.9

S5.2.2 Cell growth study

There were 6 wells in each group, which were divided into two subgroups (three wells per subgroup). Cells in one subgroup (end point study) were cultured for 7 days and media was refreshed every 2 days. Another subgroup (growth curve study) was employed for cell growth curve study using alamarBlue®, which is designed to measure quantitatively the proliferation of cells by detecting the metabolic activity.

100 µL alamarBlue® was added to each well (in the growth curve study subgroup) and incubated for 2.5 hours before the 200 µL of media with alamarBlue® was added into each well of a 96 well plate. 1ml fresh media (+ either 10% or 30% FBS) without cells were also added with 100 µL alamarBlue®. The fluorescence and absorbance of media with alamarBlue® were measured using a well plate reader every day. The fresh fluorescence and absorbance of the fresh media was the background which was subtracted from the experimental groups.

S5.3 Results

The cell growth curve and number of cells on day 7 in each group were shown in Figure S7 and Table S3.

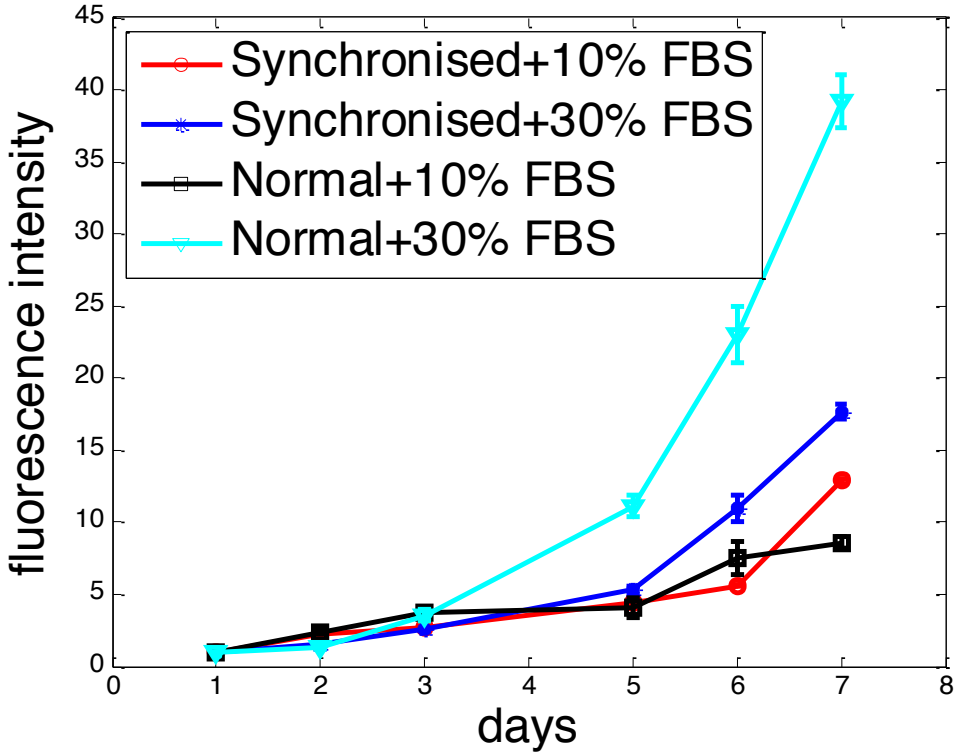

Figure S7 The normalised fluorescence intensity (± standard error of mean) of human dermal fibroblasts in 7 days. The cell number is directly proportional to the fluorescence intensity.

S6 Single HDF culture

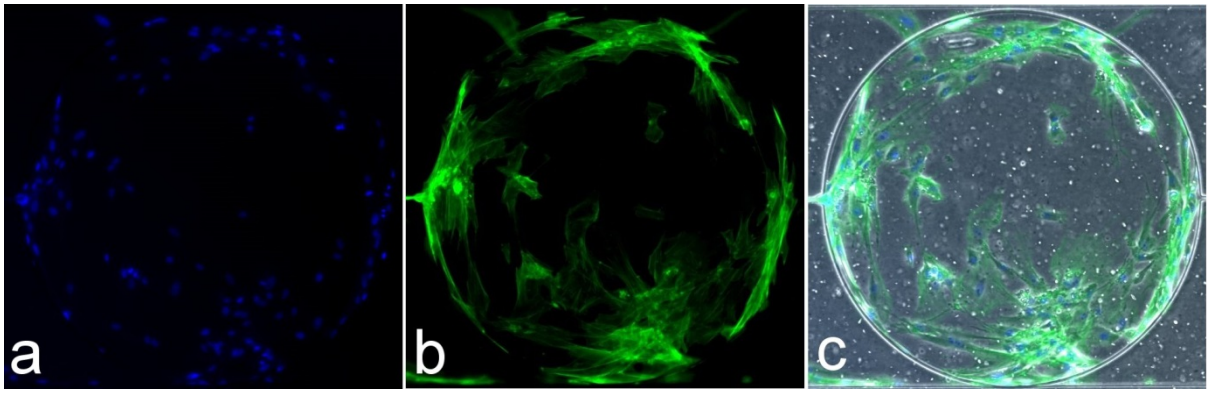

Figure S8 The nuclei (a), actin filaments (b) and the merged images (c) of the cells proliferated from a single HDF in 14 days.